Ultrafine-Grained Microstructures Evolving During Severe Plastic Deformation

T. Ungár, I. Alexandrov, and M. Zehetbauer

The microstructures of ultrafine-grained nanostructured materials developed by severe plastic deformation are widely varied in their grain size and grain-size distribution; grain boundaries and their structures; lattice defects, especially dislocations; point defects; and impurities. All of these features can be influenced by the way severe plastic deformation is applied, and thereby have decisive effects on the physical and mechanical properties of the material. Probably, the most important factors determining microstructure are the imposed stress tensor, the degree and rate of strain, the temperature of deformation, the chemical composition of the deformed material, and the type of crystal lattice, showing that in order to develop specific properties, it is crucial to understand and optimize the microstructure.

INTRODUCTION

Severe plastic deformation (SPD) can be successfully applied to obtain ultrafine-grained nanostructured materials in bulk form.[1] Recent investigations by transmission electron microscopy (TEM) and high-resolution electron microscopy (HREM) have shown that SPD-processed microstructures have not only very small grains, but also highly distorted grain boundaries[2,3] and strongly distorted crystal lattices.[4] Since one of the main sources of these distortions are dislocations, the determination of the density and distribution of dislocations is an important task in the investigation of the microstructures of SPD-processed materials.

Bragg reflections in x-ray diffraction broaden if grain or crystallite size becomes small or the material contains lattice defects, especially dislocations. In an x-ray diffraction experiment, the illuminated volume is by at least ten orders of magnitude larger than in a TEM or HREM experiment. Therefore, the statistical averages about grain size and lattice defects are far better in the x-ray experiments than in the TEM investigations. On the other hand, TEM or HREM provide specific and detailed information about the individual properties and nature, while x-ray diffraction peak profiles yield average values about densities, strains, and character of the same lattice defects. In that sense, the two methods are complementary, and the best strategy for microstructure characterization is to apply them both. The x-ray diffraction method has recently been developed to a large extent, enabling its application with more confidence.[5,6] The method has been applied successfully to characterize the microstructure in materials subjected to large deformations.[7,8]

MICROSTRUCTURES IN PLASTICALLY DEFORMED METALS

Severe plastic deformation produces fine or ultrafine grains in which the average grain dimensions approach the nanocrystalline size regime.[1] The mechanisms controlling fragmentation can be followed by studying large plastic deformations. Plastic deformation can be categorized into five different stages, where each stage corresponds to a specific behavior of the strain-hardening coefficient $\Theta = d\tau/d\gamma$, where τ and γ are the resolved shear stress and the resolved shear strain, respectively.[9] The first three stages end at a value ~1–2 for the resolved shear strain γ.[10] At the end of stage III, work hardening has a relatively low value. In stage IV, the work hardening stops decreasing and, depending on strain rate and temperature, remains constant or increases slightly with strain. Finally, in stage V, work hardening decreases and can reach zero.

After the pioneering works of Stüwe[11] and Kovács,[12] stage IV has been studied comprehensively both experimentally[9,10,13–16] and theoretically.[17–21] The experiments have shown that stage IV can be observed in most of the metals and alloys, whether hardening by dislocation accumulation and cell formation[9,10,13–16] or by planar glide without dislocation bundling and/or precipitation hardening.[16] In the case of cell-forming materials, there is general agreement that proceeding from stage III into stage IV and in stage IV the dislocation cell walls gradually become narrow, and misorientations between adjacent dislocation cells increase with deformation. There is also evidence from electrical resistivity and x-ray line broadening that the dislocation density increases steadily well into stage IV and beyond.[10,15] Detailed thermal activation analyses yielding the strain-rate sensitivity and density of thermally activated obstacles as a function of deformation suggested that hardening in stage IV is governed by the athermal storage of dislocations, while hardening in stage V is characterized by thermally driven annihilation of dislocations.[10]

Based on a special technique of high-resolution x-ray diffraction profile analysis, it has been established that in stage III, the cell-wall and cell-interior regions are put under forward and backward long-range internal stresses.[22,23] According to a simple composite model of the dislocation structure, dislocations of <100> effective Burgers vectors are lined up along the interfaces between the cell-wall and cell-interior materials in which the Burgers vectors are lying within the interface.[24] This type of dislocation structure is called polarized dipolar wall (PDW) structure[7] (a schematic model can be seen in Figure 6 in Reference 24).

In stage IV, the nature of polarization changes fundamentally.[7] The dislocations in the cell-wall material are polarized like in a small-angle grain boundary, producing an alternating tilt or twist

Table I. Data for Copper Specimens Deformed by SPD or Cold Rolling

Specimen	ρ (10^{15}m^{-2})	m (nm)	σ	d(arithmetic) (nm)	d(volume) (nm)
1x ECA	1.7	20	0.81	28	103
2x ECA	1.7	57	0.30	60	78
2x ECA + Compression	2.2	43	0.36	46	68
12x ECA	1.7	27	0.51	31	68
12x ECA + Compression	1.8	29	0.50	33	70
Cold Rolling					
$\varepsilon = 0.79$[7,15]	1.2	60	0.65	75	175
$\varepsilon = 2.45$[7,15]	1.8	33	0.32	35	45

ρ—average dislocation density; m—median deviation and σ—standard deviation of the log-normal size distribution; d(arithmetic) and d(volume)—average grain size values over the number or volume of the grains, respectively.

in the orientation of neighboring cells. This type of dislocation structure is called a polarized tilt (or twist) wall (PTW) structure[7] (a schematic model can be seen in Figure 2 in Reference 7). That kind of polarization transformation explains why and how the misorientation between adjacent dislocation cells increases so dramatically when proceeding from stage III to stage IV and is in good agreement with TEM observations.[25]

In fragmentation, this mechanism plays an important role, especially when the misoriented dislocation cells transform into ultrafine grains separated by large-angle grain boundaries. Most large-strain hardening models consider the heterogeneous dislocation cell structure as a composite of hard and soft regions where the dislocations do not interact with each other.[17–19,21] It has been shown, however, that for a successful fit of the experimental data, the deformation-induced vacancies, produced by dislocation-dislocation interaction, have to be accounted for in explaining work hardening quantitatively.[20] The fragmentation process has not yet been considered for macroscopic strengthening by most models, although first attempts were already made. The model of Argon and Haasen[19] calculates strengthening from internal stresses arising from increasing misorientation, and a new concept by Zehetbauer and Les[26] derives the macroscopic work hardening from the stresses needed to form dislocation pile-ups in front of PTW walls and/or to store additional dislocations in these walls.

X-RAY DIFFRACTION PROFILE ANALYSIS

X-ray diffraction profile analysis is one of the most powerful tools for characterizing of microstructures in plastically deformed metals and alloys. Diffraction profiles broaden when crystalline material contains lattice defects.[27] In the kinematical theory of x-ray (or neutron) scattering, it is shown that when scaling the diffraction profiles in reciprocal space coordinates, $2\sin\theta/\lambda$, instead of diffraction angles 2θ, crystallite size smallness, often called coherently scattering domains, is diffraction-order independent, whereas lattice distortions are diffraction-order dependent. The two effects can be separated, providing crystallite size and lattice distortions. The coherently scattering domains can be dislocation cells or subgrains tilted or twisted by more then a few degrees or small grains with large-angle grain boundaries. Dislocation cell-blocks can consist of several tens or hundreds of dislocation cells in which the cells have the same crystallographic orientation within one or two degrees.[9,25] In such a case, the coherently scattering domain can be several micrometers, causing no measurable size broadening, although the subgrain size can be as small as a few ten or hundred nanometers.

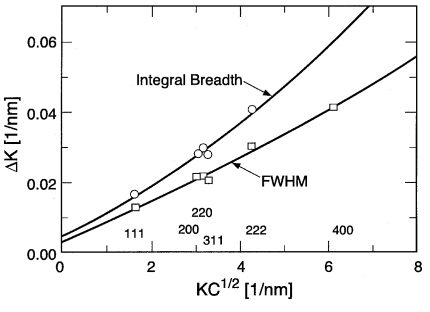

Figure 1. A typical modified Williamson-Hall plot, according to Equation 1, of the FWHMs and the integral breadths of the first six Bragg reflection profiles of a copper specimen deformed by SPD in two ECA passes.

The physical interpretation of the size obtained from line broadening requires a deep insight into the state of the material. In that context, the extension of investigations by TEM is mandatory. In a diffraction experiment, lattice distortion is given by the mean square strain $\langle\varepsilon_{L,g}^2\rangle$, where L and g are the Fourier length and the diffraction vector. The subscript g indicates that diffraction profiles sample longitudinal strains parallel to the diffraction vector. A vast amount of experimental work has shown that $\langle\varepsilon_{L,g}^2\rangle$ is almost never a constant, neither as a function of L nor as one of g. The g dependence is further complicated by the so-called strain anisotropy.[28] This means that neither the breadth nor the Fourier coefficients of the diffraction profiles are monotonous functions of the diffraction angle or g. Strain anisotropy can be well accounted for by the anisotropic contrast effect of dislocations.[5,27,29]

There are two classical procedures for the separation and evaluation of size and strain broadening—the Williamson-Hall plot[30] and the Warren-Averbach method,[31] which, however, do not take care of strain anisotropy. Modification of the two procedures has recently been suggested on the basis of the dislocation model of strain.[5] In the modified Williamson-Hall plot and the modified Warren-Averbach method, the modulus of the diffraction vector or its square, g or g^2, are replaced by $g\overline{C}^{1/2}$ or $g^2\overline{C}$, respectively, where $\overline{C}$ are the average dislocation contrast factors.[5,32,33] The modified Williamson-Hall plot can be written as[5,34]

$$\Delta K \cong 0.9/D + (\pi M^2 b^2/2)\,\rho^{1/2} K^2 \overline{C} + O(K^4 \overline{C}^2) \qquad (1)$$

where D, ρ, and b are the average particle size, the average dislocation density, and the modulus of the Burgers vector of dislocations, respectively. M is a constant depending on the effective outer cut-off radius of dislocations; for more details, see Reference 5.

A typical modified Williamson-Hall plot of the full width at half maxima (FWHM) and the integral breadths of the first six Bragg reflection profiles for one of the copper specimens investigated here (deformed by two ECA passes) is shown in Figure 1. The data follow smooth curves, which give well-defined intercepts at K = 0. Here, note that the same ΔK values reveal a strongly irregular behavior in the classical Williamson-Hall plot in a similar way as shown in Reference 5. The values of $\overline{C}$ were calculated numerically for cubic[6,32,33] and hexagonal crystal systems.[29] The $\overline{C}$ values for cubic crystals have been compiled according to a parameter q, which depends on the screw or edge character of dislocations and the elastic constants of the crystal.[6] By comparing the experimental and calculated values of the q parameter, the character of dislocations can be determined. The FWHM, the integral breadths, and the Fourier coefficients of the diffraction profiles yield three size parameters (D, d, and L_0) from which the size distribution of subgrains or small grains can be evaluated.[35] The dislocation densities are obtained from the Fourier coefficients.[5]

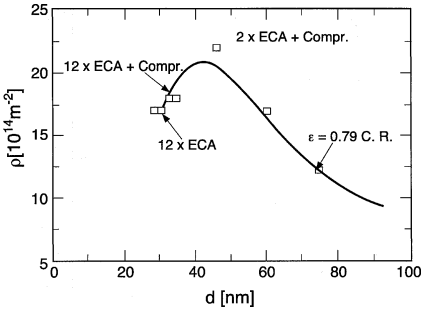

Figure 2. The average dislocation densities, ρ, as a function of the grain size averaged over the number of grains. See also Table I.

This procedure has been applied to a series of copper specimens deformed either by SPD or by cold rolling. The average dislocation densities, ρ; the median and the standard deviation, m and σ, of the log-normal crystallite size distribution; and two different averages of the grain size, one averaged over the volume and one over the number of the grains, d(volume) and d(arithmetic), are shown in Table I. Three specimens were deformed by SPD through one, two, and 12 ECA passes. Two specimens were additionally compressed by 20 percent and, for the sake of comparison, the results of two cold-rolled copper specimens are also shown in the table. The dislocation densities are plotted in Figure 2 as a function of the arithmetic average grain size. The figure suggests a lower barrier for the grain size, which cannot be overcome by SPD carried out under the present circumstances. At the same time, the dislocation density seems to reach a maximum value and even decreases when the grain size approaches the lower barrier.

TEMPERATURE-DEPENDENT X-RAY DIFFRACTION EXPERIMENTS

Static atomic displacements $\langle\mu_S^2\rangle^{1/2}$ caused by lattice defects, especially dislocations, are one of the major contributions to the mean square strain $\langle\mu^2\rangle$. The other major contributions are dynamic atomic displacements caused by the thermal motion of atoms.[36–38] The decrease of x-ray intensity due to the averaged atomic displacements $\langle\mu^2\rangle^{1/2}$ taking into account both static and dynamic atomic displacements is characterized by the Debye-Waller factor exp(–2M).[38] The parameter M is directly proportional to $\langle\mu^2\rangle$ and depends on temperature T. The Debye-Waller parameter is proportional to M and is given by

$$B = M/(\sin\theta/\lambda)^2 = 8\pi^2\langle\mu^2\rangle \qquad (2)$$

Since the nanostructured metals processed by SPD are textured,[39] a special approach was used to determine the Debye-Waller parameter.[4,40] According to this, peaks of only one family of planes, but with different orders of reflections were used (i.e., the influence of a crystallographic texture was excluded). The x-ray results for nanostructured and coarse-grained nickel showed that in both samples, the values of the Debye-Waller parameter B and the root-mean square atomic displacements $\langle\mu^2\rangle^{1/2}$ decreased linearly with decreasing temperature.

In the case of nanostructured nickel, the slope of the temperature dependence of the Debye-Waller parameter taken at the temperature interval from 295 K to 77 K was larger than in the coarse-grained sample. At each temperature, the Debye-Waller parameter of the nanostructured sample was higher than that of the coarse-grained one (e.g., at 295 K by more than a factor of two). The temperature-dependent, thermal B_T, and temperature-independent, static B_S, components of the Debye-Waller parameter were separated by the well known method that is described in Reference 41. In the case of nanostructured nickel, both values of the components of the Debye-Waller parameter significantly exceeded the values corresponding to coarse-grained nickel. This means that the defect density is increased and the character of thermal vibrations of atoms is changed due to SPD.

The Debye temperature has been determined on the basis of the Debye-Waller parameter dependence on temperature.[4] The results of calculations showed that for nanostructured nickel, the Debye temperature was 293 K, significantly smaller than the usual value for nickel equal to 375 K. One can explain the observed results taking into account the nonequilibrium character of the grain boundaries, creating long-range stress fields resulting in the increased static and dynamic atomic displacements in SPD nanostructured materials, which are especially high near grain boundaries. Here, the main reason for the observed decrease in the Debye temperature is assumed to be its reduced value in the elastically distorted near-boundary regions; whereas, inside the grain interiors it remains unchanged compared to coarse-grained samples. Such a two-phase model calculated 127 K for the Debye temperature in the near-boundary regions for nanostructured nickel, which is significantly lower, almost by 250 K, than the value for coarse-grained nickel. Analogous results were observed in the case of copper.

THE ROLE OF TEXTURE IN SPD MATERIALS

The study of crystallographic texture in nanostructured materials processed by SPD methods deserves special interest as well. The conducted investigations showed that crystallographic texture is a typical feature of SPD nanostructured materials. Axial texture was observed in pure copper processed by the SPD method of high pressure and torsion. ECA pressing resulted in the formation of a complex texture reflecting a shear character of this type of deformation.[39,42]

COMPUTER SIMULATIONS OF X-RAY DIFFRACTION PATTERNS

The x-ray diffraction patterns of SPD materials are characterized by changed integral intensities, significant broadening, long-range tails, shifted centroids of the diffraction peaks, and increased integrated diffuse background intensities.[43–47] There are a number of structural parameters that can lead to the development of such features; it is worth mentioning the small grain or crystallite size, high density and specific distribution of lattice defects, change in lattice parameter, and development of crystallographic texture. When all of these structural parameters are present at the same time it becomes difficult to interpret the patterns. There is evidence that computer simulations can be a very useful tool in solving this problem.

The x-ray diffraction patterns of nanostructured copper were simulated with a number of variable structural parameters (i.e., grain size, thickness and structure of grain boundaries, crystal lattice distortions due to long-range stress fields of extrinsic grain-boundary dislocations, and crystallographic texture).[47] Features of the experimental patterns characteristic for nanostructured materials from SPD can not be explained without considering the role of non-equilibrium grain boundaries containing a high density of the defects, creating long-range stress fields leading to large atomic displacements.

ACKNOWLEDGEMENTS

T. Ungar is grateful to the Hungarian Science Foundations for OTKA T029701 and FKFP 0116/1997. Thanks are also due to J. Gubicza and P. Hanák for their kind assistance in the x-ray diffraction work. M. Zehetbauer thanks the Austrian Science Foundation for financial support under project FWF-P12945.

References

1. R.Z. Valiev, R.K. Islamgaliev, and I.V. Alexandrov, *Progr. Mater. Sci.,* 45 (2) (2000), p. 103.
2. Z. Horita et al., *Mater. Sci. Forum,* 204-206 (1996), p. 437.
3. Z. Horita et al., *J. Mater. Res.,* 13 (1998), p. 446.
4. K. Zhang et al., *J. Appl. Phys.,* 84 (1998), p. 1924.
5. T. Ungár and A. Borbély, *Appl. Phys. Letters,* 69 (1996), p. 3173.
6. T. Ungár et al., *J. Appl. Cryst.,* 32 (1999), p. 992.
7. T. Ungár and M. Zehetbauer, *Scripta Mater.,* 35 (1996), p. 1467.
8. M. Zehetbauer et al., *Acta Mater.,* 47 (1999), p. 1053.
9. J. Gil Sevillano, P. van Houtte, and E. Aernoudt, *Progr. Mater. Sci.,* 25 (1980), p. 2.
10. M. Zehetbauer and V. Seumer, *Acta Metall. Mater.,* 41 (1993), p. 577.
11. H. P. Stüwe, *Z. Metallk.,* 56 (1965), p. 633.
12. I. Kovács, *Acta Met.,* 15 (1967), p. 1731.
13. J.M. Alberdi (Ph.D. thesis, University of Navarra, 1984).
14. D.A. Hughes, J.C. Gibeling, and W. Nix, *Proc. 7th ICSMA*, ed. H.J. McQueen et al. (Oxford, U.K.: Pergamon, 1985) p. 105.
15. M. Müller et al., *Scripta Metall. Mater.,* 35 (1996), p. 1461.
16. A.D. Rollett (Ph.D. thesis, Drexel University, 1988).
17. P. Haasen, *J. Phys. France,* 50 (1989), p. 2445.
18. D. Kuhlmann-Wilsdorf, *Mat. Sci. Eng.,* A113 (1989), p. 1.
19. A.S. Argon and P. Haasen, *Acta Metall. Mater.,* 41 (1993), p. 3289.
20. M. Zehetbauer, *Acta Metall. Mater.,* 41 (1993), p. 589.
21. Y. Estrin et al., *Acta Mater.,* 46 (1998), p. 5509.
22. H. Mughrabi et al., *Phil. Mag.,* 53 (1986), p. 793.
23. T. Ungár et al., *Phil. Mag.,* 64 (1991), p. 495.
24 H. Mughrabi, *Acta Metall.,* 31 (1983), p. 1367.
25. D.A. Hughes and N. Hansen, *Metall. Trans.,* 24A (1993), p. 2021.
26. M. Zehetbauer and P. Les, *Kovove Materialy (Metallic Materials),* 36 (1998), p. 153.
27. M.A. Krivoglaz, *Theory of X-ray and Thermal Neutron Scattering by Real Crystals* (New York: Plenum Press, 1969); *X-ray and Neutron Diffraction in Nonideal Crystals* (Berlin Heidelberg New York: Springer-Verlag, 1996).
28. P. Suortti, *The Rietveld Method,* vol. 5, ed. R.A. Young (London: Oxford University Press, 1993), pp. 167–185.
29. R. Kuzel, Jr. and P. Klimanek, *J. Appl. Cryst.,* 22 (1989), p. 299.
30. G.K. Williamson and W.H. Hall, *Acta Metall.,* 1 (1953), p. 22.
31. B.E. Warren, *Progr. Metal Phys.,* 8 (1959), p. 147.
32. T. Ungár and G. Tichy, *Phys. Stat. Sol. (a),* 171 (1999), p. 425.
33. M. Wilkens, P*hys. Stat. Sol. (a),* 104 (1987), p. K1.
34. T. Ungár and G. Ribárik, to be published.
35. T. Ungár et al., *Nanostructured Mater.,* 11 (1999), p. 103.
36. P. Debye, *Verh. Deutsch. Phys. Ges.,* 15 (1913), pp. 678, 738, 857.
37. I. Waller, *Zeitschr. Physik,* 17 (1923), p. 398.
38. B.E. Warren, *X-ray Diffraction* (Reading MA: Addison-Wesley, 1969), pp. 151–203.
39. I.V. Alexandrov et al., *Proc. Int. Conf. Textures of materials, ICOTOM-11*, ed. Z. Liang, L. Zuo, and Y. Chu Beijing: Int. Acad. Pub., 1996), p. 929.
40. S.S. Xu, *X-ray Diffraction in Metals* (Ithaca, Shanghai: Science Technical Publication Press, 1962).
41. R.W. James, *The Optical Principles of the Diffraction of X-ray* (Ithaca, NY: Cornell University Press, 1965).
42. I. Kopacz et al., to be published.
43. K. Zhang et al., *J. Appl. Phys.,* 80 (1996), p. 5617.
44. K. Zhang et al., *J. Phys. D,* 30 (1997), p. 3008.
45. K. Zhang, I.V. Alexandrov, and K. Lu, *NanoStructured Materials,* 9 (1997), p. 347.
46. I.V. Alexandrov et al., *Mater. Sci. Eng.,* A, 234-236 (1997), p. 331.
47. I.V. Alexandrov and R. Z. Valiev, *Philos. Mag. B,* 73 (1996), p. 861.

T. Ungár is with the Department of General Physics at Eötvös University Budapest. I. Alexandrov is with the Institute of Physics of Advanced Materials at Ufa State Aviation Technical University. M. Zehetbauer is with the Institute of Materials Physics at University of Vienna.

For more information, contact T. Ungár, Department of General Physics, Eötvös University Budapest, H-1518, P.O.B 32, Budapest, Hungary.